PCCP

PAPER

View Article Online
View Journal | View Issue

Particle aggregation mechanisms in ionic liquids†

Cite this: *Phys. Chem. Chem. Phys.*, 2014, **16**, 9515

Istvan Szilagyi, Tamas Szabo, Anthony Desert, Gregor Trefalt, Tamas Oncsik and Michal Borkovec*

Aggregation of sub-micron and nano-sized polystyrene latex particles was studied in room temperature ionic liquids (ILs) and in their water mixtures by time-resolved light scattering. The aggregation rates were found to vary with the IL-to-water molar ratio in a systematic way. At the water side, the aggregation rate is initially small, but increases rapidly with increasing IL content, and reaches a plateau value. This behaviour resembles simple salts, and can be rationalized by the competition of double-layer and van der Waals forces as surmised by the classical theory of Derjaguin, Landau, Verwey, and Overbeek (DLVO). At the IL side, aggregation slows down again. Two generic mechanisms could be identified to be responsible for the stabilization in ILs, namely viscous stabilization and solvation stabilization. Viscous stabilization is important in highly viscous ILs, as it originates from the slowdown of the diffusion controlled aggregation due to the hindrance of the diffusion in a viscous liquid. The solvation stabilization mechanism is system specific, but can lead to a dramatic slowdown of the aggregation rate in ILs. This mechanism is related to repulsive solvation forces that are operational in ILs due to the layering of the ILs close to the surfaces. These two stabilization mechanisms are suspected to be generic, as they both occur in different ILs, and for particles differing in surface functionalities and size.

Received 24th February 2014,
Accepted 4th April 2014

DOI: 10.1039/c4cp00804a

www.rsc.org/pccp

Introduction

Ionic liquids (ILs) have unusual properties, including high chemical stability, low vapour pressure, and a wide electrochemical window.[1–3] Their properties can also be systematically varied through the nature of their ionic constituents. Due to these unique aspects, ILs are developing into promising media for material science applications.[4–6] Among those, particle suspensions in ILs represent an important class of media, as they are relevant in catalysis,[7–11] solar cell development,[12] and mirror design.[13] Such suspensions are also obtained during the synthesis of metal,[14–16] oxide,[17,18] or latex[19] particles in ILs. The stability of such suspensions, or their aggregation state, can be decisive. The presence of aggregates further determines the suspension rheology and controls the formation of particle assemblies, colloidal glasses, and gels.[20–22] Various reports indicate that the nature of ILs and of the particles affects their aggregation state strongly. Silica particles were reported to be unstable in imidazolium-based ILs, while their stabilization could be achieved by surface functionalization.[23] Metal and silica particles were reported to be stable in dry ILs, while small amounts of water induced aggregation.[15,16,24] The presence of alkali metal cations was shown to stabilize particles in ILs.[25] However, this knowledge remains sketchy, and a mechanistic picture of particle aggregation in ILs is lacking.

The Derjaguin, Landau, Verwey, and Overbeek (DLVO) theory was developed to explain the stability of aqueous particle suspensions.[21,23,26,27] This theory represents the interaction potential as a superposition of van der Waals and electric double-layer forces, and explains why aqueous suspensions are stable at low salt levels, and unstable at higher salt levels. At low salt levels, the repulsive double-layer forces dominate and lead to slow aggregation. At higher salt levels, double-layer forces are screened, and the attractive van der Waals forces induce fast aggregation. While this behaviour is well-documented for simple salts,[28–32] a similar scenario might apply to dilute aqueous solutions of ILs.[24] The aggregation remains fast in aqueous suspensions at higher salt levels, since the diffusion is rapid due to the low viscosity of aqueous solutions. On the other hand, the high viscosity of ILs will substantially slow down the diffusion process. This effect will reduce the aggregation rate, and this mechanism will be referred to as *viscous stabilization*. The existence of highly stable particle suspensions in pure ILs contradicts DLVO theory, since the ILs should screen the double-layer forces fully.[23] Stabilization in ILs was attributed to solvation forces originating from their structuring near interfaces.[21,23,24] These forces were measured using the atomic force microscope and they were found to be oscillatory,

Department of Inorganic and Analytical Chemistry, University of Geneva, 30 Quai Ernest-Ansermet, 1205 Geneva, Switzerland.
E-mail: michal.borkovec@unige.ch; Tel: +41 22 379 6405

† Electronic supplementary information (ESI) available. See DOI: 10.1039/c4cp00804a

but overall repulsive.[24,33] This stabilization mechanism will be referred to as *solvation stabilization*.

Here we demonstrate that solvation and viscous stabilization controls the aggregation of particles in ILs. This assertion will be based on detailed measurements of aggregation rates of colloidal particles in IL–water mixtures with time-resolved light scattering. The present article provides the first systematic study of this kind, and shows that these techniques can be used to clarify the mechanisms of particle aggregation processes in ILs.

Methods

The following section summarizes the essential methods and concepts needed to analyse particle aggregation kinetics by time-resolved light scattering. The supplement provides details concerning the materials and experimental protocols used.

Particle aggregation kinetics

Particles suspended in a liquid diffuse due to thermal motion, and attractive van der Waals forces make them stick upon contact. When the suspension is initially composed of isolated particle monomers, they will form aggregates, initially dimers, according to the scheme

$$A + A \rightarrow A_2 \tag{1}$$

The kinetics of this process can be described using the rate equation

$$-\frac{dN_1}{dt} = 2 \cdot \frac{dN_2}{dt} = kN_1^2 \tag{2}$$

where N_1 and N_2 are the number concentrations of the monomers and dimers, respectively, t is the time, and k is the aggregation rate coefficient. Eqn (2) describing aggregation of colloidal particles is exactly the same as in chemical reaction kinetics, except in that field one defines the rate coefficient half as large. The other important difference from the chemical kinetics is that colloidal particles readily form higher order aggregates, such as trimers, tetramers, namely

$$\begin{aligned} A_2 + A &\rightarrow A_3 \\ A_3 + A &\rightarrow A_4 \\ A_2 + A_2 &\rightarrow A_4 \\ &\cdots \end{aligned} \tag{3}$$

Therefore, aggregates keep growing, until they sediment, cream, or interlink to form a gel. By assuming that each of these elementary kinetic steps proceeds with the same rate coefficient k, Smoluchowski has shown that in a suspension initially composed of monomers only, the total number of particles or aggregates $N = N_1 + N_2 + N_3 + \ldots$ decreases as[26,27]

$$N = \frac{N_0}{1 + t/T_{1/2}} \tag{4}$$

where N_0 is the total (or initial) particle concentration $N_0 = N_1 + 2N_2 + 3N_3 + \ldots$ and

$$T_{1/2} = \frac{2}{kN_0} \tag{5}$$

is the half-time of aggregation. This half-time represents the characteristic time, after which the total number of aggregates is reduced by a factor of two. When only monomers and dimers are present, eqn (2) would lead to the same expression for $T_{1/2}$ as eqn (5) up to the factor of 2.

The van der Waals attraction close to contact is normally very strong, which makes the aggregation process irreversible, meaning that aggregated particles do not detach from each other. For weaker attraction forces, as for example, in the case of depletion interactions or critical Casimir forces, the aggregation process may become reversible and lead to equilibrium phase separation.[34–36] Currently, we have no indications that such a situation might be encountered in ILs. Therefore, the irreversible aggregation process always leads to destabilization of a colloidal suspension, whereby the half-time given by eqn (5) sets the corresponding time scale. Depending on the system, however, this half-time may differ by orders of magnitude. When this half-time is large, the suspension is stable, while when it is small, it is unstable. For a half-time that is comparable to the experimental time window, the aggregation process can be followed by various techniques in real time. Initially, particle dimers form, while higher order aggregates occur later (Fig. 1). Correspondingly, one refers to *early stages* and *late stages* of the aggregation. Since the formation of doublets in eqn (1) is a second order kinetic process, the half-time does not only depend on the aggregation rate coefficient k, but also on the particle number concentration N_0. Thus, a suspension can be stabilized by adjusting the conditions such that aggregation rate coefficient is small, by appropriate dilution, or both.

In the case of fast aggregation, one assumes that the diffusing particles do not interact but they stick to each other at every encounter.[26] This model is equivalent to diffusion controlled reaction kinetics or, in colloid language, to a fast aggregation process. Smoluchowski has further shown that the corresponding rate coefficient is given by[26,27]

$$k_S = 16\pi D_1 R_1 = \frac{8k_B T}{3\eta} = 1.23 \times 10^{-17}\ \mathrm{m^3\ s^{-1}} \tag{6}$$

where by D_1 and R_1 denote the diffusion coefficient and the radius of the aggregating particles. The second equality sign in eqn (6) follows from the Stokes–Einstein relation, which relates the former quantities as[26]

$$D_1 = \frac{k_B T}{6\pi\eta R_1} \tag{7}$$

where η is the shear viscosity of the dispersing liquid, T is the absolute temperature, and k_B is the Boltzmann constant. The numerical value given in eqn (6) refers to water at 25 °C, while for ILs this value can be substantially smaller.

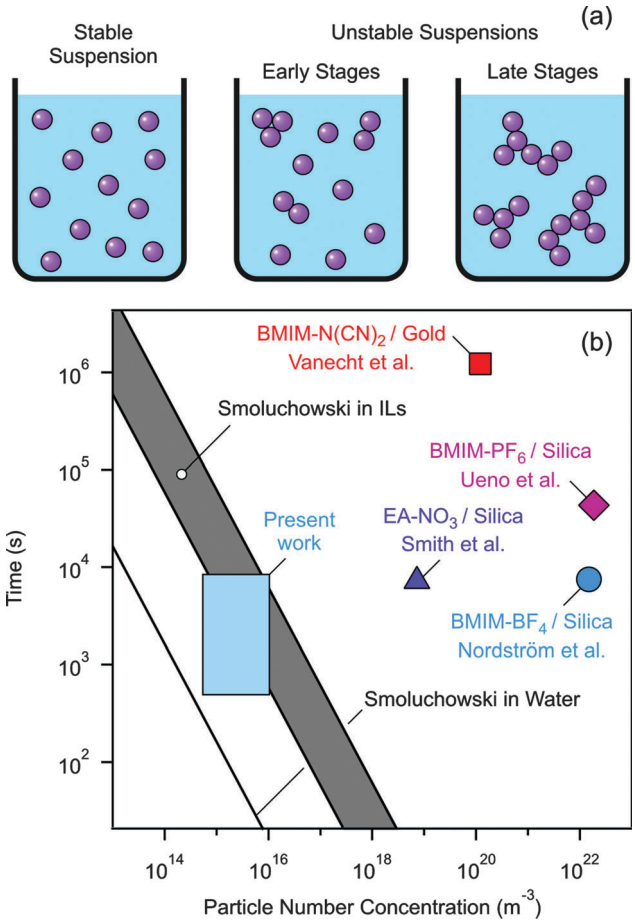

Fig. 1 Particle aggregation in ILs. (a) Schemes depicting the structure of a stable suspension and of unstable suspensions at early and late stages of the aggregation. (b) Aggregation time scale *versus* the particle number concentration. Half-times are calculated using eqn (5) and Smoluchowski's eqn (6) in water (solid line) and in the ILs used in the present study (shaded area). The blue region indicates the conditions of the present experiments. Data points refer to experimental time windows reported by Nordström *et al.*,[25] Smith *et al.*[24] involving ethylammonium ions (EA^+), Vanecht *et al.*,[16] and Ueno *et al.*[23] The other acronyms are defined in Fig. 2 and further details are given in Table S6 (ESI†).

Eqn (5) and (6) can be used to distinguish stable and unstable colloidal particle suspensions in aqueous salt solutions (Fig. 1b). Since viscosities of ILs can be substantially larger than the ones of aqueous solutions,[5,6] the respective boundary is displaced to the right. The stability time windows and the corresponding particle concentrations for stable particle suspensions in ILs reported in the literature are also shown.[16,23–25] The fact that these points cluster above the grey region suggests the importance of solvation stabilization. When the interaction potential acting between the particles is known, aggregation rates could be estimated more accurately.[26,37] We shall not pursue this aspect here, since the information concerning the interaction potentials between particles in ILs is currently incomplete.

Light scattering

Particle suspensions are being routinely characterized by static light scattering (SLS) and dynamic light scattering (DLS).[26,38] When these techniques are employed in a time-resolved fashion, they allow probing particle aggregation processes in detail.[39–42]

SLS measures the light scattering intensity I *versus* the scattering angle θ, which is commonly expressed in terms of the magnitude of the scattering vector

$$q = \frac{4\pi n}{\lambda_0}\sin\frac{\theta}{2} \tag{8}$$

where n is the refractive index of the medium and λ_0 is the wavelength of the incident light in vacuum. The scattering intensity $I(q)$ from a stable and dilute suspension of colloidal particles can be used to evaluate the particle size accurately. For small particles and weak contrast, the angular dependence of the scattering intensity can be calculated within the Rayleigh, Gans, and Debye (RGD) approximation. The contrast is characterized by the difference between the refractive indices of the particles and the dispersing liquid. In the general case, the exact Mie theory for spheres must be used.[43] For quantitative analysis, particle polydispersity and back-reflection correction have to be included.

The scattering intensity from an aggregating suspension varies with time. For a dilute suspension, this quantity can be expressed as

$$I(q,t) = I_1(q)N_1(t) + I_2(q)N_2(t) + \ldots \tag{9}$$

where $I_1(q)$ and $I_2(q)$ are the scattering intensities of the monomer and dimer, respectively. For early stages of aggregation, one can measure the initial apparent static rate Σ, which reflects the rate of change of the scattering intensity normalized by the initial intensity. This quantity can be obtained from eqn (2) and (9) and reads[40]

$$\Sigma = \frac{1}{I(q,0)}\cdot\left.\frac{\mathrm{d}I(q,t)}{\mathrm{d}t}\right|_{t\to 0} = kN_0\left(\frac{I_2(q)}{2I_1(q)} - 1\right) \tag{10}$$

In order to evaluate the aggregation rate coefficient, the optical factor must be known. Within the RGD approximation, this factor is given by[26,40]

$$\frac{I_2(q)}{2I_1(q)} = 1 + \frac{\sin(2qR_1)}{2qR_1} \tag{11}$$

In the general case, the T-matrix theory must be used to evaluate the ratio of scattering intensities.[37,43] At low scattering angles ($q \to 0$), the apparent static rate is always positive, meaning that the scattering intensity increases with time. At larger angles, this quantity can also become negative, which reflects the fact that the scattering intensity may also decrease with time.

DLS measures the intensity autocorrelation function, and from its decay constant one can extract the apparent diffusion coefficient D. In a stable suspension, the particle radius can be directly evaluated from this quantity using the Stokes–Einstein equation (eqn (7)). When a dilute suspension aggregates, the apparent diffusion coefficient can be expressed as[40]

$$D(q,t) = \frac{D_1 I_1(q)N_1(t) + D_2 I_2(q)N_2(t) + \ldots}{I_1(q)N_1(t) + I_2(q)N_2(t) + \ldots} \tag{12}$$

where D_1 and D_2 correspond to the diffusion coefficients of the monomers and dimers, respectively. We prefer to report the apparent hydrodynamic radius $R(q,t)$ that is obtained from the apparent diffusion coefficient $D(q,t)$ using eqn (7). In the early stages of aggregation one can measure the apparent dynamic rate Δ, which corresponds to the initial relative rate of change of the apparent hydrodynamic radius normalized to the initial radius. Following similar arguments as above, this rate can be expressed as[40]

$$\Delta = \frac{1}{R(q,0)} \cdot \left.\frac{\mathrm{d}R(q,t)}{\mathrm{d}t}\right|_{t\to 0} = kN_0\left(1-\frac{1}{\alpha}\right)\frac{I_2(q)}{2I_1(q)} \qquad (13)$$

where $\alpha = D_1/D_2 = R_2/R_1 \simeq 1.39$ is the hydrodynamic factor. The respective hydrodynamic radii of the monomer and the dimer are denoted as R_1 and R_2. The numerical value of this factor α can be estimated from low Reynolds number hydrodynamics.[44] This apparent dynamic rate is always positive, meaning that the hydrodynamic radius always increases with time, as one would intuitively expect. As will be shown in the next section, these light scattering techniques are a powerful means to investigate particle aggregation processes in ILs.

Results and discussion

Aggregation of sub-micron sulphate and amidine latex particles, as well as nano-sized sulphate latex particles, was studied in various ILs and their mixtures with water (Fig. 2a). Many ILs are hygroscopic, and may contain substantial amounts of water.[45] We have therefore systematically studied particle suspensions over a wide range of IL-to-water molar ratios, from dilute solution of ILs in water (water side) to ILs containing small amounts of water (IL side). We have analysed ILs containing the anions tetrafluoroborate, BF_4^-, dicyanamide, $N(CN)_2^-$, and thiocyanate, SCN^-, with 1-butyl-3-methylimidazolium, $BMIM^+$, as the cation. We have further investigated ILs with $N(CN)_2^-$ as the anion, and $BMIM^+$, 1-butyl-3-methylpyridinium dicyanamide, $BMPY^+$, and 1-butyl-1-methylpyrrolidinium, $BMPL^+$ as cations. Comparison experiments were carried out with 1-butylpyridinium tetrafluoroborate, BPY-BF_4, and simple KCl electrolyte solutions. Viscosities, refractive indices, and densities of the IL–water mixtures were determined by standard techniques (Fig. 2b and Fig. S1, ESI†). The viscosities of pure ILs used are 30–150 times larger than the one of water. Refractive indices and densities can be accurately described by ideal mixing laws. We will first summarize how light scattering can be used to characterize these particles and their aggregation kinetics. Subsequently, we will discuss the generic dependence of the aggregation rates on the IL-to-water molar ratio, and finally address system specificities.

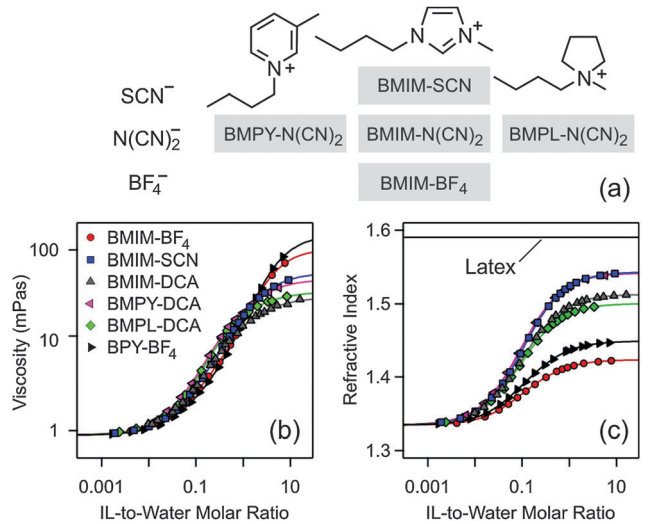

Fig. 2 Properties of ILs used and of their mixtures with water. (a) Structures and abbreviations, (b) shear viscosity, (c) and refractive index measured at 533 nm. The refractive index of the latex particles is also indicated.

Particle characterization by light scattering

We study spherical polystyrene latex particles as model particles. Most experiments were carried out with sub-micron particles having amidine surface modification and a radius of 110 nm and with sulphate surface modification and a radius of 265 nm. Fig. 3a shows measured form factors of the particles in water and in BMIM-SCN whereby the scattering intensity originating from pure ILs was subtracted. This residual scattering can be up to 10 times larger than the one for toluene, probably due to the presence of nm-sized transient clusters that are spontaneously forming in the ILs.[46] However, this residual scattering is still sufficiently small such that the excess scattering from the particles can be easily measured. The form factors are compared with best fits with Mie theory, whereby the refractive index of 1.59 was used for polystyrene.[47] Analogous results of the simpler RGD calculations are also shown. One observes that

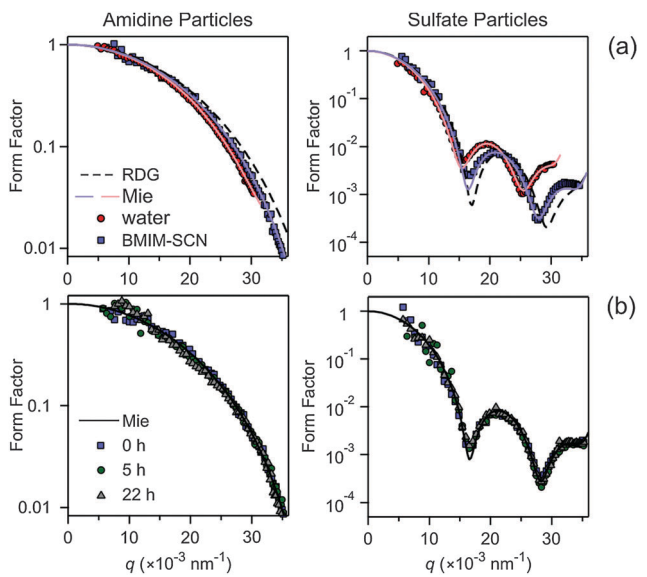

Fig. 3 Monomer form factors $P(q)$ *versus* the magnitude of the scattering vector q of amidine latex particles of 110 nm in radius (left) and sulphate latex of 265 nm (right). (a) The experimental points in water and in pure BMIM-SCN are compared with Mie and RGD theory from which the particle radius can be extracted. (b) No dependence with time of the form factors is observed in BMIM-SCN.

the RGD theory is applicable in ILs, while deviations from this theory are apparent in water, especially for the larger sulphate particles. Mie theory must be used in that case. The fitted particle radii and polydispersities are in excellent agreement with the values obtained by electron microscopy (Table S1, ESI†). RGD theory works well in the IL since the contrast is smaller, meaning that the refractive index of the latex particle is closer to the one of the IL than the one of water (Fig. 2c). Fig. 3b further illustrates that the form factor of the latex particles remains the same over long times. The constancy of this scattering profile confirms that the particles remain stable in the IL and that they neither swell nor dissolve. Hydrodynamic radii were also measured by DLS in these suspensions and they are about 6% larger than the ones obtained by SLS (Table S1, ESI†). This slight increase in radius is probably caused by polydispersity effects or solvation of the surface layer. The absolute scattering intensity remains constant within the experimental error of about 5% over the entire experimental time period, which further demonstrates that sedimentation or creaming effects are negligible in these systems.

Aggregation rates by time-resolved light scattering

The scattering intensity from an aggregating suspension may increase or decrease with time (Fig. 4a). The initial slope of this intensity trace reflects the apparent static rate Σ given in eqn (10) and this quantity can be determined by fitting a straight line to the initial part of the time-dependent scattering intensities. When the scattering intensity decreases with time, this quantity becomes negative. The measured dependence of the apparent static rate Σ on the magnitude of the scattering vector q is compared in Fig. 5a with predictions of RGD theory. This relation agrees well with the experiment for the amidine particles, but the more accurate T-matrix theory must be used for sulphate latex. The deviations are more important in water than in the IL due to larger contrast. The remaining discrepancies are probably related to slight particle asphericity. The respective aggregation rates are obtained by least-squares fit (Table 1). One observes that the aggregation rates in ILs are substantially smaller than the ones in water.

In an aggregating suspension, the apparent hydrodynamic radius always increases with time (Fig. 4b). The apparent dynamic rate Λ can be obtained by fitting straight lines to the initial portion of the hydrodynamic radius trace. The dependence of the apparent dynamic rate Λ on the magnitude of the scattering vector q can be fitted well with eqn (13) whereby the optical factor can be determined by RGD or T-matrix theory (Fig. 5b). When one uses the aggregation rate coefficients obtained from static light scattering, one obtains the hydrodynamic factors. They are summarized in Table 1 and they agree well with the theoretical value of $\alpha = 1.39$. The data points scatter more strongly in the IL due to weaker contrast.

When the optical and hydrodynamic factors are known, the aggregation rate coefficients can also be obtained from the measurement of the apparent dynamic rate at a specific scattering angle. The typical procedure is to perform time-resolved single-angle DLS experiments at various compositions and determine the apparent dynamic rates from the initial slope (Fig. 4c and d).

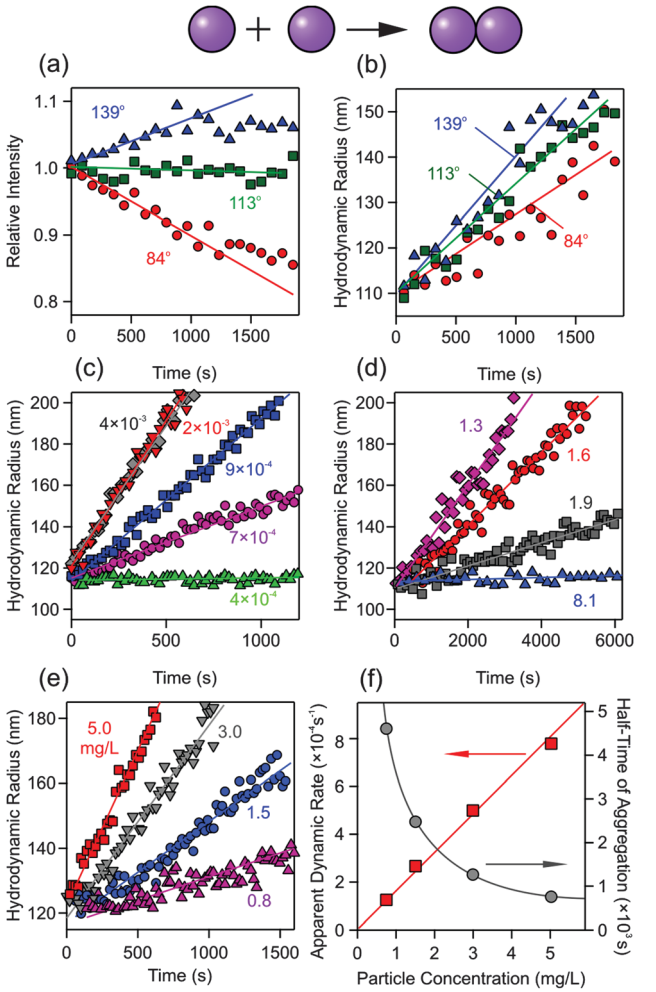

Fig. 4 Time-dependence of the light scattering signal in aggregating particle suspensions in ILs. Amidine latex particles measured at different scattering angles in BMIM-SCN of 0.092 IL-to-water molar ratio with (a) SLS and (b) DLS. Hydrodynamic radius measured using DLS for amidine latex particles in BPY-BF_4–water mixtures at different IL-to-water molar ratios (c) on the water side and (d) on the IL side. Particle concentration dependence for amidine latex particles in BPY-BF_4 on the (e) hydrodynamic radius and (f) the apparent dynamic rate (left axis) and half-time of aggregation (right axis).

The rate coefficients can be extracted from eqn (13) by inserting the known values of the optical and hydrodynamic factors. This single-angle DLS technique was used to measure the rate coefficients in the various IL–water mixtures, and the resulting aggregation rates are in excellent agreement with multi-angle SLS (Table 1).

In order to probe the doublet formation rate, the experiment must be carried out in the early stages of aggregation. This condition can be ensured with time-resolved DLS by satisfying two criteria. First, the initial apparent hydrodynamic radius should agree within experimental error with the corresponding radius in a stable suspension. Second, the relative increase of the apparent radius should be not more than 20–30% of its initial value. Such conditions are best found by varying the particle concentration (Fig. 4e). This figure also indicates that

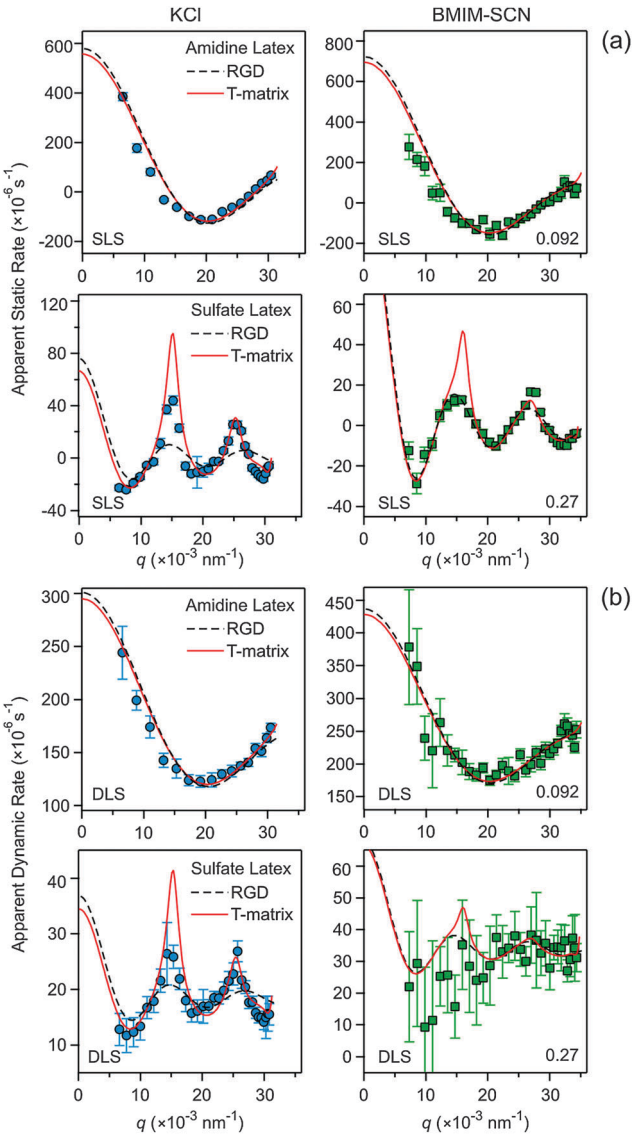

Fig. 5 Apparent aggregation rates *versus* the magnitude of the scattering vector q of amidine and sulphate latex particles measured in 1.0 M KCl (left column) and in BMIM-SCN water mixtures of the IL-to-water molar ratios indicated (right column). Experimental data are compared with RGD (dashed line) and T-matrix (solid line) calculations. The resulting aggregation rates and hydrodynamic factors are given in Table 1. (a) SLS and (b) DLS.

the apparent rate of aggregation is proportional to the particle concentration (Fig. 4f), as stipulated by eqn (13).

Another way to ensure that one focuses on the early stages of the aggregation process is to evaluate the half-time of the aggregation (Fig. 4f). These half-times are also shown in Fig. 1. Since our aim is to measure aggregation rates, we situate ourselves near the unstable region. The appropriate experimental window must be substantially shorter than the half-times, in practice by about a factor 3–5. To estimate the half-time properly, the actual aggregation rate coefficient must be known. However, this quantity is only accessible when the respective light scattering measurements have been completed and not when the experiment is initiated. From this point of view, the criteria concerning the relative increase of the hydrodynamic radius are more practical.

Generic features

Fig. 6a shows the measured aggregation rates for the different latex particles in various ILs and in their water mixtures. The striking aspect is that all systems studied behave similarly. Three main aggregation regimes can be identified. (i) At low IL-to-water ratios, one recovers the classical DLVO regime. In this regime, the aggregation rate increases strongly with the IL content first, and then saturates at a plateau value. The increase in the rate corresponds to slow aggregation, which results from progressive screening of the double-layer repulsion. The plateau reflects fast aggregation, where particle encounters are only limited by their rapid diffusion in water. (ii) At higher IL-to-water ratios, the aggregation rate decreases gradually. This decrease originates from the increasing viscosity, even though the aggregation process remains diffusion controlled. In the systems studied, this mechanism can slow down the aggregation process by almost two orders of magnitude. This regime is referred to as *viscous stabilization*. (iii) At high IL-to-water ratios, which correspond to ILs containing small amounts of water, the aggregation rate decreases rapidly with increasing IL content. This regime reflects stabilization that is specific to the type of the IL, and will be referred to as *solvation stabilization*.

The DLVO regime (i) on the water-rich side is very similar to simple, monovalent salts, like KCl. This fact is not surprising since ILs normally dissociate in water like simple, strong electrolytes.[48] The effect of simple salts on the aggregation of colloidal particles is well documented.[30–32] The transition between slow and fast aggregation can be described by DLVO theory for weakly charged particles.[30,31] Slow aggregation for highly charged particles is often more rapid than predicted

Table 1 Aggregation rates and hydrodynamic factors of sub-micron latex particles measured using time-resolved light scattering

	Amidine latex[a]		Sulphate latex[b]	
Method	KCl[c]	BMIM-SCN[d]	KCl[c]	BMIM-SCN[d]
Multi-angle SLS[e]	$(2.9 \pm 0.1) \times 10^{-18}$	$(8.5 \pm 0.5) \times 10^{-19}$	$(3.3 \pm 0.1) \times 10^{-18}$	$(4.5 \pm 0.9) \times 10^{-19}$
Multi-angle DLS[f]	1.35 ± 0.02	1.43 ± 0.02	1.32 ± 0.02	1.35 ± 0.02
Single-angle DLS[e]	$(3.1 \pm 0.3) \times 10^{-18}$	$(8.3 \pm 0.8) \times 10^{-19}$	$(3.2 \pm 0.2) \times 10^{-18}$	$(3.0 \pm 0.4) \times 10^{-19}$

[a] Amidine latex of 110 nm in radius. [b] Sulphate latex of 265 nm in radius. [c] Measurements were carried out in 1.0 M KCl solutions. [d] IL-to-water molar ratios of 0.092 and 0.27 were used for amidine and sulphate latexes, respectively. [e] Aggregation rate coefficients k in $m^3\ s^{-1}$. [f] Measured hydrodynamic factor α.

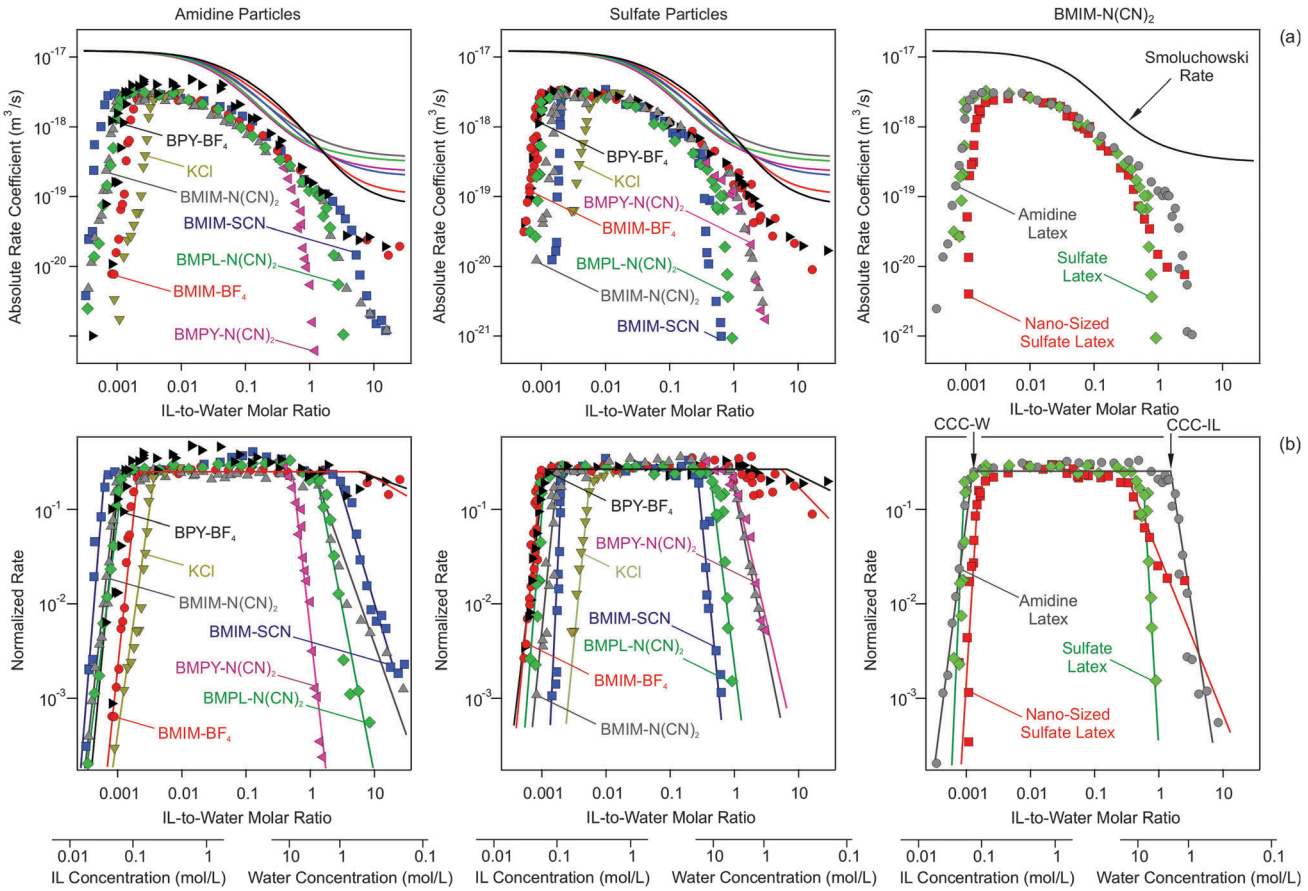

Fig. 6 Aggregation rates of sub-micron latex particles *versus* the IL-to-water molar ratio in various ILs. Molar IL and water concentrations are indicated on separate axes. Amidine (left column) and sulphate latex (middle column) in different ILs, and different particles in BMPL-N(CN)$_2$ with the CCCs indicated for the amidine particles. (a) Aggregation rate coefficient k and (b) the same quantity normalized to the Smoluchowski rate coefficient k_S. Solid lines in (a) correspond to the Smoluchowski rate, while in (b) they serve to guide the eye.

by DLVO theory, which is typically caused by surface charge heterogeneities.[30,32,49]

The importance of viscous stabilization in regime (ii) can be confirmed by comparing the aggregation rate coefficients to the Smoluchowski's value k_S given in eqn (6). Viscosities of the IL–water mixtures increase strongly with increasing IL content (Fig. 2b), and thus the Smoluchowski's rate decreases (Fig. 6a). This point can be better illustrated by plotting the aggregation rate coefficients normalized with the Smoluchowski's value k/k_S (Fig. 6b). The normalized rate coefficient remains constant throughout the entire intermediate concentration regime (ii) within experimental error, which confirms that the aggregation is diffusion controlled. However, the rate coefficient is about a factor of 2–4 smaller than the Smoluchowski's value. Similar discrepancies were reported in aqueous suspensions of latex, silica, or metal oxide particles.[49–52] They can be partly explained by including van der Waals and hydrodynamic interactions in the calculation of the aggregation rate, which results in aggregation rates that are about a factor of two smaller than the Smoluchowski's value. While the Hamaker constant, which defines the strength of the van der Waals force, could vary with the type of IL and its water content, the actual value of the aggregation rate depends only weakly on this constant.[27] The remaining discrepancies probably originate from inaccuracies in the hydrodynamic resistance function at small distances.[52]

The onset of solvation stabilization can be best localized through the abrupt decrease of the normalized rate coefficient at high IL content (Fig. 6b). Solvation stabilization occurring in regime (iii) on the IL-rich side is probably caused by repulsive forces generated by the structuring of the ILs near solid surfaces. This structuring was observed by X-ray reflectivity,[53] and the respective forces could be measured using the surface forces apparatus[54] and the atomic force microscope.[24,33,55] While such solvation forces are oscillatory, they are overall repulsive, and probably responsible for the stabilization of colloidal particles in ILs as suggested earlier.[21] Since we lack reliable models of the interaction potential acting between the particles in IL–water mixtures, we shall not attempt to evaluate the aggregation rates in this regime quantitatively.

The transition between slow and fast aggregation within the DLVO regime at the water rich side occurs in a narrow concentration range, referred to as the critical coagulation concentration (CCC). A similar critical concentration can be identified at the IL rich side, which signals the transition between the solvation and viscous stabilization regime. We distinguish

these two CCCs by referring to CCC-W on the water-rich side, and by CCC-IL on the IL-side. To remain in line with the customary definition of CCC in water, we will express CCC-W as molar concentration of the IL. In analogy, CCC-IL will be expressed as molar concentration of water. The respective molar concentration axes are indicated in Fig. 6. Fig. S2–S4 (ESI†) facilitate conversions to these and other concentration units. The respective CCCs can be inferred from Fig. 6 and they are summarized in Table S5 (ESI†).

Sub-micron amidine latex particles

CCC-W is lower for the ILs than for the simple salts, such as KCl. Charged particles suspended in simple, monovalent salt solutions have CCCs in the range of 0.1–0.5 M.[28,29,56] The corresponding values induced by ILs are consistently lower, around 0.03–0.1 M. This shift is probably related to a stronger affinity of the IL anions to the particle surface than with Cl^-. One further observes that CCC-W increases in the sequence of SCN^-, $N(CN)_2^-$, and BF_4^-, suggesting that the affinity of the surface for these anions decreases in the same way. The effect of the cations on CCC-W is less pronounced.

The CCC-IL can be clearly observed for all ILs studied, except in the presence of the BF_4^- anion. Typical values observed reflect water concentrations of 2–7 M. The ILs containing the BF_4^- anion seem to induce only minor solvation stabilization for the water contents studied, eventually setting in below 1.0 M. This hypothesis seems to be consistent with the absence of aggregation of gold particles in very dry BMIM-BF_4 over time periods that were substantially larger than the half-times estimated using the Smoluchowski relation (Fig. 1b).[16] Silica suspensions were also found to be unstable in BMIM-BF_4.[23] Adopting this hypothesis, CCC-IL increases in the sequence of BF_4^-, SCN^-, and $N(CN)_2^-$. The effect of cations seems to be more important for CCC-IL, since $BMPY^+$ yields the highest value, while $BMIM^+$ and $BMPL^+$ behave similarly.

Sub-micron sulphate latex particles

The values of CCC-W for the sulphate particles are very similar to the values for the amidine particles. This fact can be understood since the magnitudes of the charge densities of both types of particles are comparable (Table S1, ESI†). However, the effects of anions are different. With the $BMIM^+$ cation, one observes the reverse sequence to the amidine particle. The CCC-W thus increases through the anions BF_4^-, $N(CN)_2^-$, and SCN^-. This trend suggests that the affinity of the surface for these anions decreases in the same sequence, and is thus opposite to the one for amidine particles. This reversed trend is probably related to the negative charge of these particles. The effect of cations on CCC-W is again minor, and these values are similar for $BMIM^+$, $BMPL^+$, and BPY^+.

The CCC-IL for the sulphate particles situates in the range 3–13 M, which is somewhat larger than for the amidine particles. As for the amidine particles, the ILs containing the BF_4^- anions lead only to minor suspension stabilization at low water concentrations, around 0.4 M. The CCC-IL increases with BF_4^-, $N(CN)_2^-$, and SCN^-, which reflects the same sequences observed at the water side. The role of cations is less important, one still observes the sequence $BMPY^+$, $BMIM^+$, and $BMPL^+$. These findings suggest again that cations interact with the particle surfaces more weakly than anions.

Nano-sized sulphate latex particles

To address the applicability of our findings to smaller particles, aggregation rates of nano-sized sulphate latex particles with 50 nm radius in BMPL-$N(CN)_2$ and its water mixtures were measured (Table S1, ESI†). Due to the weak scattering power of these particles, the respective measurements are more difficult, especially in ILs. While the overall trends are similar, the present data suggest that the nano-sized particles aggregate more slowly than the sub-micron sized ones on the IL side. This point is in agreement with the observation that suspensions of nano-sized silica particles were more stable than suspensions of larger ones.[21] However, such differences could also be related to different particle concentrations of the samples.

The present scenario is consistent with visual observations of silica particle suspensions in mixtures of ethylammonium nitrate and water by Smith *et al.*[24] These suspensions were stable in pure water and the pure IL, but unstable in the mixtures. Fig. 1 reveals that solvation stabilization must be the relevant stabilization mechanism in that system too. We thus estimate CCC-W to be around 0.1 M and CCC-IL to be around 2 M in that system.

Conclusions

Our light scattering studies demonstrate that colloidal particles suspended in ILs and their water mixtures form aggregates. However, the time scale of this process strongly depends on the particle concentration and on the value of the aggregation rate coefficient. The rate coefficients vary characteristically. At the water side, ILs behave like simple, monovalent salts and the data are in line with the DLVO theory. In this DLVO regime, one observes slow aggregation at low IL content. With increasing IL content, the aggregation rate increases and finally reaches the plateau reflecting fast aggregation. At the IL side, aggregation may proceed again very slowly. Two mechanisms are responsible for this stabilization. The *viscous stabilization* mechanism is important in viscous ILs, and originates from the slowdown of the diffusion process in a viscous liquid. The *solvation stabilization* mechanism is system specific, but can lead to a dramatic slowdown of the aggregation rate. This mechanism is probably related to repulsive solvation forces that are operational in ILs due to strong layering close to surfaces. These two stabilization mechanisms are suspected to be generic, as they are operational in different ILs and for particles with different surface functionalities and of different size. We further suspect that in ILs containing BF_4^- anions the principal mechanism is viscous stabilization, and solvation stabilization is unimportant, unless the IL is extremely dry. On the other hand, ILs containing $N(CN)_2^-$ or SCN^- anions tend to stabilize suspensions by both mechanisms, and solvation stabilization can be even operational in ILs containing 10% of water by mass.

Acknowledgements

Financial support by the Swiss National Science Foundation, Swiss Scientific Exchange Program and the University of Geneva is gratefully acknowledged.

References

1 A. P. Abbott and K. J. McKenzie, *Phys. Chem. Chem. Phys.*, 2006, **8**, 4265–4279.
2 M. Armand, F. Endres, D. R. MacFarlane, H. Ohno and B. Scrosati, *Nat. Mater.*, 2009, **8**, 621–629.
3 F. Endres and S. Z. El Abedin, *Phys. Chem. Chem. Phys.*, 2006, **8**, 2101–2116.
4 N. V. Plechkova and K. R. Seddon, *Chem. Soc. Rev.*, 2008, **37**, 123–150.
5 H. Tokuda, K. Hayamizu, K. Ishii, M. Abu Bin Hasan Susan and M. Watanabe, *J. Phys. Chem. B*, 2004, **108**, 16593–16600.
6 H. Tokuda, K. Hayamizu, K. Ishii, M. A. B. H. Susan and M. Watanabe, *J. Phys. Chem. B*, 2005, **109**, 6103–6110.
7 M. Ruta, G. Laurenczy, P. J. Dyson and L. Kiwi-Minsker, *J. Phys. Chem. C*, 2008, **112**, 17814–17819.
8 J. D. Scholten, B. C. Leal and J. Dupont, *ACS Catal.*, 2012, **2**, 184–200.
9 F. T. Li, X. J. Wang, Y. Zhao, J. X. Liu, Y. J. Hao, R. H. Liu and D. S. Zhao, *Appl. Catal., B*, 2014, **144**, 442–453.
10 X. Yang, Z. F. Fei, D. B. Zhao, W. H. Ang, Y. D. Li and P. J. Dyson, *Inorg. Chem.*, 2008, **47**, 3292–3297.
11 S. Shylesh, D. Hanna, S. Werner and A. T. Bell, *ACS Catal.*, 2012, **2**, 487–493.
12 P. Wang, S. M. Zakeeruddin, P. Comte, I. Exnar and M. Gratzel, *J. Am. Chem. Soc.*, 2003, **125**, 1166–1167.
13 E. F. Borra, O. Seddiki, R. Angel, D. Eisenstein, P. Hickson, K. R. Seddon and S. P. Worden, *Nature*, 2007, **447**, 979–981.
14 H. Itoh, K. Naka and Y. Chujo, *J. Am. Chem. Soc.*, 2004, **126**, 3026–3027.
15 L. L. Lazarus, C. T. Riche, N. Malmstadt and R. L. Brutchey, *Langmuir*, 2012, **28**, 15987–15993.
16 E. Vanecht, K. Binnemans, S. Patskovsky, M. Meunier, J. W. Seo, L. Stappers and J. Fransaer, *Phys. Chem. Chem. Phys.*, 2012, **14**, 5662–5671.
17 Y. Zhou and M. Antonietti, *J. Am. Chem. Soc.*, 2003, **125**, 14960–14961.
18 M. Ramalakshmi, P. Shakkthivel, M. Sundrarajan and S. M. Chen, *Mater. Res. Bull.*, 2013, **48**, 2758–2765.
19 H. Minami, K. Yoshida and M. Okubo, *Macromol. Rapid Commun.*, 2008, **29**, 567–572.
20 Q. M. Ji, S. Acharya, G. J. Richards, S. L. Zhang, J. Vieaud, J. P. Hill and K. Ariga, *Langmuir*, 2013, **29**, 7186–7194.
21 K. Ueno and M. Watanabe, *Langmuir*, 2011, **27**, 9105–9115.
22 S. S. Moganty, S. Srivastava, Y. Y. Lu, J. L. Schaefer, S. A. Rizvi and L. A. Archer, *Chem. Mater.*, 2012, **24**, 1386–1392.
23 K. Ueno, A. Inaba, M. Kondoh and M. Watanabe, *Langmuir*, 2008, **24**, 5253–5259.
24 J. A. Smith, O. Werzer, G. B. Webber, G. G. Warr and R. Atkin, *J. Phys. Chem. Lett.*, 2010, **1**, 64–68.
25 J. Nordström, L. Aguilera and A. Matic, *Langmuir*, 2012, **28**, 4080–4085.
26 W. B. Russel, D. A. Saville and W. R. Schowalter, *Colloidal Dispersions*, Cambridge University Press, Cambridge, 1989.
27 M. Elimelech, J. Gregory, X. Jia and R. A. Williams, *Particle Deposition and Aggregation: Measurement, Modeling, and Simulation*, Butterworth-Heinemann Ltd., Oxford, 1995.
28 T. Lopez-Leon, A. B. Jodar-Reyes, D. Bastos-Gonzalez and J. L. Ortega-Vinuesa, *J. Phys. Chem. B*, 2003, **107**, 5696–5708.
29 D. N. Furlong, A. Launikonis, W. H. F. Sasse and J. V. Sanders, *J. Chem. Soc., Faraday Trans. 1*, 1984, **80**, 571–588.
30 S. H. Behrens, M. Borkovec and P. Schurtenberger, *Langmuir*, 1998, **14**, 1951–1954.
31 M. Kobayashi, M. Skarba, P. Galletto, D. Cakara and M. Borkovec, *J. Colloid Interface Sci.*, 2005, **292**, 139–147.
32 N. Ryde and E. Matijevic, *J. Chem. Soc., Faraday Trans.*, 1994, **90**, 167–171.
33 R. Hayes, G. G. Warr and R. Atkin, *Phys. Chem. Chem. Phys.*, 2010, **12**, 1709–1723.
34 V. J. Anderson and H. N. W. Lekkerkerker, *Nature*, 2002, **416**, 811–815.
35 A. Zaccone, J. J. Crassous and M. Ballauff, *J. Chem. Phys.*, 2013, **138**, 104908.
36 D. Bonn, J. Otwinowski, S. Sacanna, H. Guo, G. Wegdam and P. Schall, *Phys. Rev. Lett.*, 2009, **103**, 156101.
37 W. Lin, M. Kobayashi, M. Skarba, C. Mu, P. Galletto and M. Borkovec, *Langmuir*, 2006, **22**, 1038–1047.
38 B. J. Berne and R. Pecora, *Dynamic Light Scattering*, Robert E. Krieger Publishing, Malabar, 1990.
39 D. A. Weitz, J. S. Huang, M. Y. Lin and J. Sung, *Phys. Rev. Lett.*, 1984, **53**, 1657–1660.
40 H. Holthoff, S. U. Egelhaaf, M. Borkovec, P. Schurtenberger and H. Sticher, *Langmuir*, 1996, **12**, 5541–5549.
41 S. H. Xu and Z. W. Sun, *Soft Matter*, 2011, **7**, 11298–11308.
42 P. Sandkuhler, M. Lattuada, H. Wu, J. Sefcik and M. Morbidelli, *Adv. Colloid Interface Sci.*, 2005, **113**, 65–83.
43 M. I. Mishchenko, L. D. Travis and A. A. Lacis, *Scattering, Absorption, and Emission of Light by Small Particles*, University Press, Cambridge, 2002.
44 W. L. Yu, E. Matijevic and M. Borkovec, *Langmuir*, 2002, **18**, 7853–7860.
45 E. J. Gonzalez, A. Dominguez and E. A. Macedo, *J. Chem. Eng. Data*, 2012, **57**, 2165–2176.
46 S. Chen, S. Zhang, X. M. Liu, J. Wang, J. Wang, K. Dong, J. L. Sun and B. Xu, *Phys. Chem. Chem. Phys.*, 2013, **16**, 5893–5906.
47 X. Y. Ma, J. Q. Lu, R. S. Brock, K. M. Jacobs, P. Yang and X. H. Hu, *Phys. Med. Biol.*, 2003, **48**, 4165–4172.
48 M. Bester-Rogac, A. Stoppa, J. Hunger, G. Hefter and R. Buchner, *Phys. Chem. Chem. Phys.*, 2011, **13**, 17588–17598.
49 M. Schudel, S. H. Behrens, H. Holthoff, R. Kretzschmar and M. Borkovec, *J. Colloid Interface Sci.*, 1997, **196**, 241–253.

50 S. H. Behrens, D. I. Christl, R. Emmerzael, P. Schurtenberger and M. Borkovec, *Langmuir*, 2000, **16**, 2566–2575.
51 M. Kobayashi, F. Juillerat, P. Galletto, P. Bowen and M. Borkovec, *Langmuir*, 2005, **21**, 5761–5769.
52 P. Sinha, I. Szilagyi, F. J. Montes Ruiz-Cabello, P. Maroni and M. Borkovec, *J. Phys. Chem. Lett.*, 2013, **4**, 648–652.
53 M. Mezger, H. Schroder, H. Reichert, S. Schramm, J. S. Okasinski, S. Schoder, V. Honkimaki, M. Deutsch, B. M. Ocko, J. Ralston, M. Rohwerder, M. Stratmann and H. Dosch, *Science*, 2008, **322**, 424–428.
54 R. G. Horn, D. F. Evans and B. W. Ninham, *J. Phys. Chem.*, 1988, **92**, 3531–3537.
55 J. J. Segura, A. Elbourne, E. J. Wanless, G. G. Warr, K. Voitchovsky and R. Atkin, *Phys. Chem. Chem. Phys.*, 2013, **15**, 3320–3328.
56 W. Lin, P. Galletto and M. Borkovec, *Langmuir*, 2004, **20**, 7465–7473.

